Electron-phonon interactions in the Andreev bound states of aluminum nanobridge Josephson junctions

James T. Farmer, Azarin Zarassi, Sadman Shanto, Darian Hartsell, and Eli M. Levenson-Falk

Phys. Rev. B **107**, L140506 — Published 27 April 2023

DOI: 10.1103/PhysRevB.107.L140506

Electron-phonon interactions in the Andreev Bound States of aluminum nanobridge Josephson junctions

James T. Farmer,* Azarin Zarassi, Sadman Shanto, Darian Hartsell, and Eli M. Levenson-Falk†
Department of Physics, University of Southern California and
Center for Quantum Information Science and Technology, University of Southern California
(Dated: March 21, 2023)

We report continuous measurements of quasiparticles trapping and clearing from Andreev Bound States in aluminum nanobridge Josephson junctions integrated into a superconducting-qubit-like device. We find that trapping is well modeled by independent spontaneous emission events. Above 80 mK the clearing process is well described by absorption of thermal phonons, but other temperature-independent mechanisms dominate at low temperature. We find complex structure in the dependence of the low-temperature clearing rate on the Andreev Bound State energy. Our results shed light on quasiparticle behavior in qubit-like circuits.

Non-equilibrium quasiparticles (QPs) in superconducting quantum circuits can hinder device operation, limiting coherence in most qubit architectures [1, 2] and inducing correlated, difficult-to-correct errors across multiple qubits on the same chip [3, 4]. The QPs are generated by non-thermal mechanisms such as pair-breaking infrared photons [5] or energy dissipation from local radioactivity and cosmic rays [2]. Significant non-equilibrium QP populations with fractional densities $x_{qp} \sim 10^{-9} - 10^{-5}$ are ubiquitously observed [5–8] and have proven difficult to eliminate. Mitigation strategies such as improved light-tight shielding [5], input/output filtering with infrared absorbers [7, 9, 10], and device engineering [11–17] have reduced QP densities over the last decade. Many works have probed QP populations by detecting single charge tunneling across Josephson junctions [1, 7, 15, 18–22] or observing QPs trapped inside the Andreev Bound States (ABS) of a junction [23–27]. These ABS provide a complementary measurement of QP behavior, and can be used as qubit modes themselves [28, 29]. In many implementations the ABS qubit relies on a non-equilibrium QP trapping in order to initialize the state; such qubits are vulnerable to additional trapping events and to accidental clearing of the QP from the ABS. There is thus a great need to better understand the behavior of QPs in ABS and the mechanisms for QPs transitions between ABS and bulk continuum states.

In this letter we investigate the electron-phonon interactions involved in trapping a quasiparticle into / clearing a quasiparticle from an Andreev Bound State. We show continuous, real-time measurements of ABS trapping dynamics as a function of ABS energy and device temperature in a superconducting-qubit-like device. We find that QP trapping is consistent with independent spontaneous emission events from a bulk QP population that is a combination of a temperature-independent non-equilibrium background and a thermal equilibrium density. We further find that QP clearing from an ABS is consistent with a process dominated by absorption of a thermal phonon at temperatures above 80 mK. At low temperatures, we find evidence that absorption of microwave photons by trapped QPs is the dominant clearing mechanism, even at low drive powers. We analyze the mean QP occupancy of our ABS device and find independent confirmation of our trapping and clearing models. Our results shed light on quasiparticle behavior in ABS and in qubit-like circuits in general.

To study QP trapping, we require a circuit element which is sensitive to the occupation of single electron states with tunability below the superconducting gap. We find such an element in the aluminum nanobridge Josephson junction, an all-superconducting junction which was shown [30–32] to follow the KO-1 current-phase relation [33] while providing several hundred conduction channels. Each conduction channel hosts a pair of ABS with energies

$$E_A(\delta) = \pm\Delta\sqrt{1 - \tau \sin\frac{\delta}{2}} \tag{1}$$

measured from the Fermi energy. The transparency τ is the probability that an incident Cooper pair is transmitted across the junction and δ is the phase bias across the junction; Δ is the superconducting gap. For short ($\lesssim 100$ nm) aluminum nanobridges, τ approximately follows a Dorokhov distribution with a strong preference to be 0 or 1 [31, 34]. When occupied, each ABS in a given channel carries equal and opposite contributions to the supercurrent. The negative state is usually occupied while the positive state is unoccupied. However, the positive ABS dips below the gap Δ when both δ and τ are nonzero, making it energetically favorable for a quasiparticle above the gap (i.e. in the bulk continuum) to relax into the ABS and become trapped. When this occurs the supercurrent contribution of the given channel is cancelled and the channel is "poisoned". This is the mechanism of our detection: the Josephson inductance becomes a function of the number of trapped quasiparticles.

By embedding a DC SQUID with symmetric aluminum nanobridge junctions in a $\lambda/4$ coplanar waveguide resonator, we are able to measure the trapping of a QP as a

* jtfarmer@usc.edu
† elevenso@usc.edu

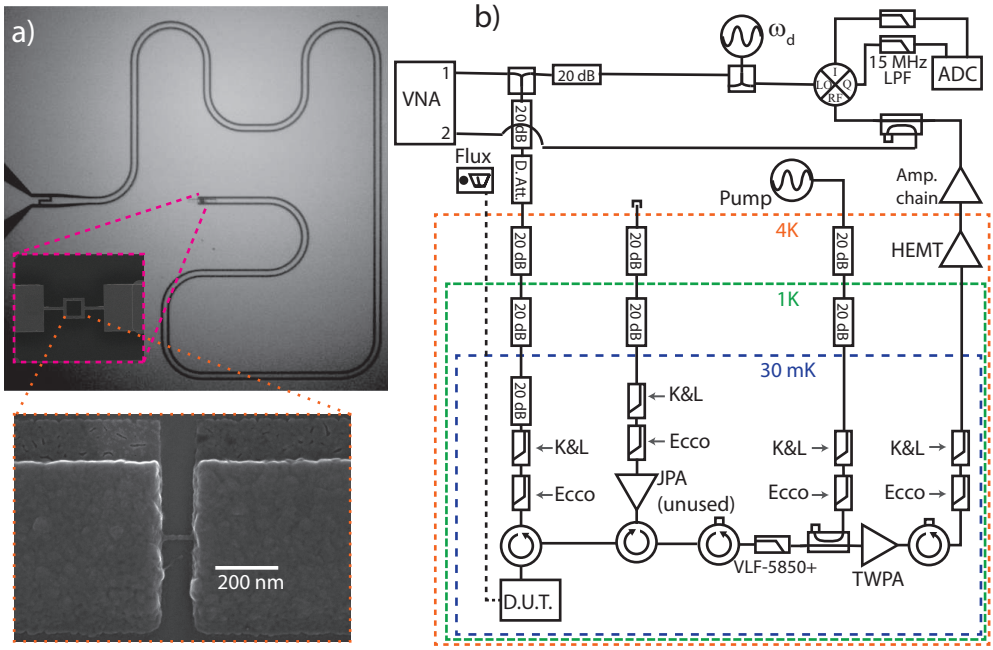

FIG. 1. (a) Images of similar device: a $\lambda/4$ resonator is grounded through a DC SQUID with a pair of symmetric aluminum nanowire junctions. These junctions are approximately 25 nm × 8 nm × 100 nm. (b) The readout drive ω_d is generated at room temperature and attenuated along the path through the dilution refrigerator to the base stage. At 30 mK, pair breaking photons on all inputs and outputs are reduced by K&L 12 GHz low pass filters and Eccosorb CR110 infrared absorbers. The signal circulates to reflect off our device and pass through a 5.85 GHz low pass filter. The signal is then amplified by a travelling wave parametric amplifier (TWPA) whose pump is inserted via a directional coupler. The signal exits the dilution refrigerator receiving further amplification by a HEMT at 4K and a series of low noise amplifiers at room temperature. The signal is homodyne demodulated by an IQ mixer and the resulting quadratures are digitized after 15 MHz low pass filtering. A Keithley Sourcemeter sends DC current along the dashed path to a coil in the device package and a VNA is used to measure the resonance as a function of flux.

resonant frequency shift of the resonator. This allows for a high bandwidth, continuous measurement of the ABS occupation in a qubit-like circuit using a standard dispersive measurement setup [27]. A constant flux bias on the SQUID introduces a constant, symmetric phase bias to the junctions $\delta = \pi\phi$ (where ϕ is the applied flux in units of flux quanta), tuning the ABS energies. The fundamental mode $f_0(\phi)$ of our resonator is flux tunable from 4.301 GHz to $\tilde{4}$.25 GHz with a linewidth $\kappa = 2\pi \times 250$ kHz and the shift due to trapping a single quasiparticle $\chi(\phi)/2\pi$ ranges from 100 kHz to 400 kHz. A device image and wiring diagram are shown in Fig. 1.

We perform continuous microwave reflection measurements on our device which is mounted in a dilution refrigerator with a base temperature of 30 mK. The reflected signal is homodyne demodulated with an IQ mixer and the two quadratures of signal are recorded as a gapless voltage record in 3 s segments by an Alazar 9371 digitizer operating at 300 MHz sample rate. This is down sampled to 1 MHz sample rate to ensure sufficient SNR for our later analysis; low-power data sometimes requires further downsampling to maintain an SNR greater than 3. Data was collected and processed in this way over a range of parameters: the dilution refrigerator temperature, the ABS energy, and the applied microwave power. For brevity, we restrict ourselves in this analysis to a constant power of -133 dBm ($\sim$ 25 photons) at the device. This power was chosen as it gives reasonable SNR at all flux values, but is always at least 6 dB below the power at which we start to observe a power-dependent resonant frequency shift due to the nonlinearity of the nanoSQUID inductance [32]. More details on data collection are given in the Supplement [35].

We take the downsampled IQ voltage record and fit it to a Hidden Markov Model (HMM) [36, 37]. The HMM fits the data to two modes with Gaussian-distributed voltage emissions, corresponding to the "hidden" state of the resonance with 0 or 1 trapped QPs. While there is evidence of periods when there are 2 trapped QPs, these are rare enough that they do not affect the analysis, and so we neglect them [27]. The HMM also fits a matrix of transition rates between hidden states, assuming a Markovian process of switching between states. These transition rates are parameters of the model and are used in the majority of our analysis. The fit modes and transition matrix are then used in a maximum a posteriori probability estimation procedure to assign a hidden state to every data point. Our HMM uses the Viterbi algorithm to perform this estimation, finding the series of hidden states that is most likely to generate the

observed data. Thus we use the HMM to transform the IQ voltage time series into time series of the number of trapped QPs (either 0 or 1 in this analysis) and we obtain the rates of QPs trapping and clearing from the HMM fit. A more detailed explanation is given in the Supplement [35].

The present work explores the behavior of three quantities derived from HMM analysis as a function of ABS energy and temperature. Γ_{trap} is the rate of QPs relaxing from the bulk into available ABS of the junction, $\Gamma_{release}$ is the rate of clearing QPs from ABS to the bulk, and $\bar{n}$ which we call the mean occupation is the time average of the number of trapped QPs. Γ_{trap} and $\Gamma_{release}$ are found from the off-diagonal elements of the HMM transition matrix—that is, they are parameters of the model used to extract the ABS occupation time series—while $\bar{n}$ is found from averaging the extracted QP occupation time series over the full 3 second record.

We begin our modeling with the trap rate. Assuming trapping events are independent of each other and spontaneous emission dominates the QP relaxation into the ABS, each QP in the bulk has a temperature-independent trapping rate. This implies the overall trap rate is separable: $\Gamma_{trap}(\Delta_A, T) = f(\Delta_A)x(T)$, where $x(T)$ is the fractional quasiparticle density and $\Delta_A \equiv \Delta - E_A$ is the trap depth. We take the limit $\tau \to 1$ as the Dorkhov distribution $\rho(\tau)$ is sharply peaked at 0 and 1, and channels with 0 transmittivity do not contribute to the transport. The fractional quasiparticle density should be the sum of a non-equilibrium background x_{ne} and a thermal population:

$$x(T) = x_{ne} + \sqrt{\frac{2\pi k_B T}{\Delta}} \exp\left(\frac{-\Delta}{k_B T}\right). \tag{2}$$

We expect that most bulk QPs are near the gap energy, so for spontaneous emission we take $f(\Delta_A) \propto \Delta_A^3$. Putting this together, we obtain a model for the trap rate

$$\Gamma_{trap} = \beta \Delta_A^3 \left(x_{ne} + \sqrt{\frac{2\pi k_B T}{\Delta}} \exp\left(\frac{-\Delta}{k_B T}\right)\right) \tag{3}$$

where β, Δ, and x_{ne} are the free parameters. To improve the quality of our fit, we take advantage of the low temperature saturation of trap rate $\Gamma^0_{trap}(\Delta_A) \approx \beta \Delta_A^3 x_{ne}$ for $T \leq 120$ mK. We first subtract $\Gamma^0_{trap}(\Delta_A)$ from Eq. 3 and fit the resulting quantity to find the gap Δ and scaling factor β. Next we divide Eq. 3 by $\Gamma^0_{trap}(\Delta_A)$ and fit this normalized rate with the fractional non-equilibrium density x_{ne} as the only free parameter. This fitting procedure is covered in detail in the supplement [35]. In Figure 2, we show the full model (Eq. 3) using the combined results of this fitting procedure. We find $\beta = 8.73 \pm 0.68 \times 10^{15}$ MHz/eV^3, $x_{ne} = 8.50 \pm 0.10 \times 10^{-7}$, and $\Delta = 185.0 \pm 1.5 \mu$eV. We note that the fractional non-equilibrium density x_{ne} is quite high compared to recent works [2, 7, 8] which show a fractional density on the order of 10^{-9}. Our setup uses light-tight radiation shields

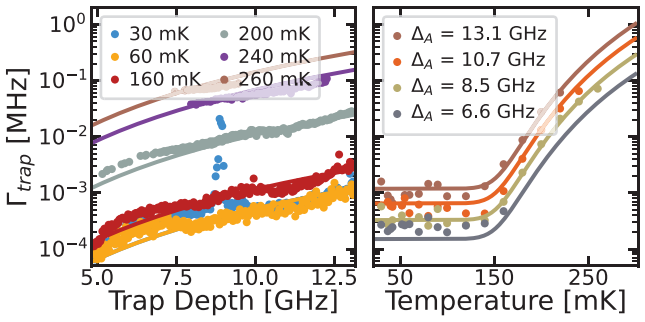

FIG. 2. Measured trap rate (circles) and model (solid lines). The dependence on the trap depth Δ_A is shown on the left, while temperature dependence is shown on the right. We note the peak in 30 mK data around 9 GHz on the left was observed as a period of significantly larger than normal mean occupation which lasted approximately 1 hour in laboratory time. The source of this peak has not been found and it is not reproducible.

on all stages of the fridge, with Berkeley Black infrared-absorbing coating [38] on the interior of the 100 mK and mixing chamber shields. In addition, the sample package is mounted inside of an Amumetal 4K shield with a tin-plated copper can nested inside, also with a Berkeley Black interior coating. We use custom-made Eccosorb filters as well as K&L 12 GHz low-pass filters on all inputs and outputs. A full diagram is available in shown in Fig. 1. We suspect that our device geometry may contribute to the higher-than-expected density, as large areas of low-gap superconducting aluminum are galvanically coupled to the SQUID. It also may be the case that our filtering is insufficient, as recent results have shown evidence that even very extensive filtering does not fully remove stray infrared light [39]. We see no significant dependence of the trapping rate on the drive power, and so it is unlikely that our drive is generating additional QPs.

The left panel of Figure 2 shows a peak in the 30 mK data near 9 GHz. This anomaly was present in the trap rate and mean occupation, while the release rate was marginally increased. We attribute this to a temporary increase in the bulk QP density, as repeated measurement under nearly identical conditions did not show this effect. The period of increased trapping lasted for approximately one hour with no change in fridge conditions and no obvious environment factors to blame. We note the duration of the effect is too long to be caused by adhesive strain [40] or a strong cosmic ray [41].

We now turn our attention to $\Gamma_{release}$. To promote a trapped QP from ABS to the continuum of states above the gap, sufficient energy (at least Δ_A) must be absorbed. In a well shielded dilution refrigerator, we expect this energy to come from the absorption of phonons. The clearing rate due to electron-phonon interactions should be linear in the phonon density,

$$\Gamma_{phonon}(\Delta_A, T) \propto \rho_{\epsilon \geq \Delta_A}(T), \tag{4}$$

where $\rho_{\epsilon\geq\Delta_A}(T)$ is the density of phonons with energy exceeding the trap depth. In the supplement [35], we integrate the Debye density of states and Bose-Einstien distribution over energies exceeding the trap depth to obtain the model for QP clearing due to phonons:

$$\Gamma_{phonon}(\Delta_A, T) = \alpha T^3 \left[-\left(\frac{\Delta_A}{k_B T}\right)^2 \ln\left(1 - e^{\frac{-\Delta_A}{k_B T}}\right) + \frac{2\Delta_A}{k_B T}\mathrm{Li}_2\left(e^{\frac{-\Delta_A}{k_B T}}\right) + 2\mathrm{Li}_3\left(e^{\frac{-\Delta_A}{k_B T}}\right)\right]. \quad (5)$$

In the above, $\mathrm{Li}_n(x)$ is the polylogarithm function of order n and $\alpha = C_{ABS\to bulk} k_B^3/2\pi^2\hbar^3\nu^3$ is an overall scaling factor; ν is the speed of sound in our sample and $C_{ABS\to bulk}$ relates the ABS clearing rate to the phonon density. The formal foundation for $C_{ABS\to bulk}$ is a matter worthy of study as it represents the coupling between ABS and an incoherent bath.

In our measurements, we observe that the release rate saturates at $T \leq 60$ mK to a value which depends on the power of our microwave readout tone, suggesting that low-temperature clearing is dominated by driven electron-photon interactions. This is surprising because a single readout photon (≈ 4.27 GHz) has insufficient energy to clear the ABS trap ($\Delta_A(\phi) > 5$ GHz $\forall$ measured ϕ). It may be the case that nonlinear processes in the resonator or transitions to intermediate ABS mediate this process, which will be the subject of future work. Accounting for this readout-dominated electron-photon clearing, we can model the total release rate as

$$\Gamma_{release}(\Delta_A, T) = \Gamma_{RO}(\Delta_A) + \Gamma_{phonon}(\Delta_A, T), \quad (6)$$

where the electron-photon clearing rate Γ_{RO} is the subject of future work. For now, we take advantage of the low temperature saturation $\Gamma^0_{release} \approx \Gamma_{RO}$ to eliminate this photon contribution and maintain focus on the electron-phonon clearing rate. Our model is

$$\Gamma_{release}(\Delta_A, T) - \Gamma^0_{release}(\Delta_A) \approx \Gamma_{phonon}(\Delta_A, T) \quad (7)$$

which is equivalent to the right hand side of Eq. 5. We keep $\Delta = 185\mu$eV and fit Eq. 7 with α as the only free parameter as shown in Figure 3. We obtain $\alpha = 38.51 \pm 0.36$ MHz/K^3. Clearly the high temperature release rate is dominated by a thermal distribution of phonons, but this result shows that non-thermal sources may dominate at typical qubit operating temperatures. We point out that the 240 mK and 260 mK data in the top left panel show some clipping of the release rate data to the 1 MHz sample rate – A limitation of our measurement rather than a physical effect.

Our last feature of interest is the mean occupation $\bar{n}$, which is taken directly from the extracted time series of ABS occupations, not from HMM parameters. We start with a simple sum over weighted probabilities:

$$\bar{n} = \sum_i iP(i), \quad (8)$$

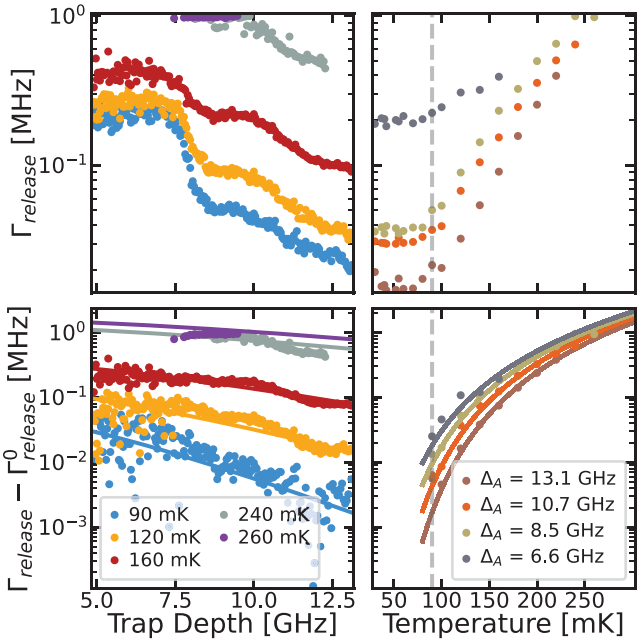

FIG. 3. (top) The measured release rate vs trap depth and temperature. The top left panel shows structure in the trap depth dependence which is attributed to the driven electron-photon interactions which dominate at low temperature. In the top right panel, the low temperature saturation is visible. The grey dashed line indicates the cutoff temperature (90 mK) for the fit. (bottom) The measured release rate minus the low temperature saturation is shown as circles, while the phonon clearing model (Eq. 7) is shown as solid curves.

where $P(i)$ is the probability of having i trapped QPs. In this analysis, we are only distinguishing between 1 trapped QP and 0 trapped QPs, as the incidence of 2 or more trapped QPs is quite rare. We can therefore assume a stationary distribution to obtain

$$P(0)\Gamma_{trap} = P(1)\Gamma_{release}. \quad (9)$$

Plugging (9) into (8), we obtain the model for the mean occupation:

$$\bar{n}(\Delta_A, T) = P(0)\frac{\Gamma_{trap}(\Delta_A, T)}{\Gamma_{release}(\Delta_A, T)}. \quad (10)$$

Unfortunately, we are unable to eliminate the driven electron-photon contribution as we did in Eq. (7) so

we simply leave $\Gamma_{RO}(\Delta_A)$ as a free parameter and fit each line cut along temperature separately. We normalize by dividing out the low-temperature saturation ($T \leq 60$ mK) to obtain the model

$$\|\bar{n}_{\Delta_A}(T)\| = \frac{1 + \frac{1}{x_{ne}}\sqrt{\frac{2\pi k_B T}{\Delta}} e^{\frac{-\Delta}{k_B T}}}{1 + \alpha_M T^3 \left[-\left(\frac{\Delta_A}{k_B T}\right)^2 \ln\left(1 - e^{\frac{-\Delta_A}{k_B T}}\right) + \frac{2\Delta_A}{k_B T}\mathrm{Li}_2\left(e^{\frac{-\Delta_A}{k_B T}}\right) + 2\mathrm{Li}_3\left(e^{\frac{-\Delta_A}{k_B T}}\right)\right]}. \tag{11}$$

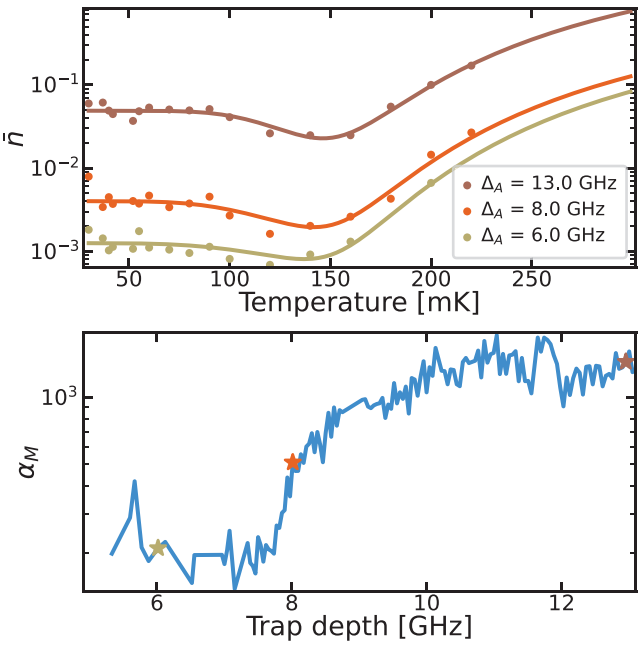

FIG. 4. (top) The measured mean occupation (circles) and the corresponding fit (solid) are shown against temperature. Note that a different fit is performed at each value of Δ_A. (bottom) The fit parameter α_M vs trap depth. Stars indicate the value of α_M for the three curves of the same color displayed in the top panel.

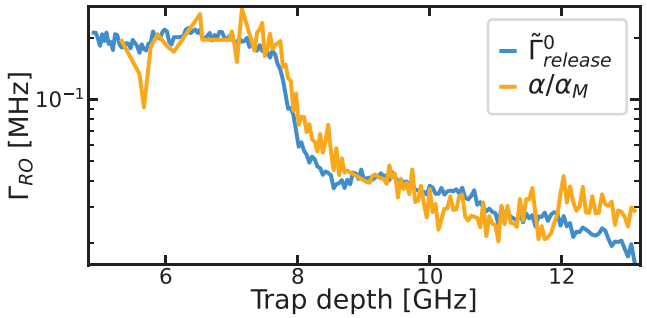

FIG. 5. Two sources of estimate for the rate of readout photons clearing QPs from the ABS traps. The measured low temperature release rate (blue) and the fit parameter from the mean occupation, shown as α/α_M (orange), where $\alpha = 38.51$ is found from fitting the phonon contribution to the release rate as shown in Figure 3. We point out that these agree in shape and magnitude despite coming from different sources.

We fit this independently for each trap depth, while holding $x_{ne} = 8.5 \times 10^{-7}$ and $\Delta = 185\mu$eV fixed. The only fit parameter is $\alpha_M \equiv \alpha/\Gamma_{RO}(\Delta_A)$. The results are shown in Figure 4. We note the characteristic dip in mean occupation for $T \in [80, 150]$ mK arises from an increased phonon population leading to faster clearing of ABS, while the rise for $T \geq 150$ mK is due to large population of thermal QPs.

We may check for self-consistency in our description by examining the relationship between $\alpha_M(\Delta_A)$ and the driven electron-photon clearing rate $\Gamma_{RO}(\Delta_A)$. We directly measure $\Gamma_{RO}(\Delta_A)$ as the low-temperature saturation of the release rate and compare this with the estimate obtained from α/α_M, as shown in Figure 5. Note that the former quantity comes entirely from the HMM parameters, while the latter quantity comes from direct analysis of the ABS occupation time series. These quantities agree very closely, indicating that our analysis is robust. The driven electron-photon clearing rate has significant structure in its dependence on Δ_A which is repeatable. There is additional structure when one looks at the dependence on the microwave power, which is the focus of our future work with this system.

By utilizing the many ABS of aluminum nanobridge Josephson junctions, we are able to measure and explain the behavior of quasiparticle trapping in qubit-like circuits over a range of trap depth and temperature. We show that QPs relax into traps primarily by spontaneous emission of a phonon. The close agreement between our data and our model suggests that most QPs entering the trap are originally at or near the superconducting gap Δ. This indicates that any "hot" non-equilibrium quasiparticles are first relaxing to the gap in an independent process before trapping or that the majority of non-equilibrium quasiparticles exist at the gap edge, in agreement with past results [42]. We do not see any evidence of "photon-assisted trapping" (in analogy to the photon-assisted tunneling observed in tunnel junctions) where an infrared photon breaks a Cooper pair, promoting a QP directly into an ABS. This process may occur at lower rates, and is the subject of future work. We also show that clearing of QPs from ABS traps at temperatures above 90 mK occurs primarily through absorption of phonons which are distributed according to the Debye

model. Other sources, such as microwave photons, are the dominant source of ABS-clearing energy at qubit operating temperatures. Our results further elucidate the behavior of equilibrium and non-equilibrium quasiparticles in superconducting circuits.

ACKNOWLEDGMENTS

We thank Leonid Glazman for useful discussions and the MIT Lincoln Laboratory for providing the TWPA used in these measurements. This work was funded by the AFOSR under FA9550-19-1-0060 and the NSF under DMR-1900135. JF, AZ, DH fabricated the device. JF, AZ, SS performed measurements. JF and AZ performed the analysis. JF wrote the manuscript with input from all authors. ELF was the PI supervising all aspects of the work.

[1] K. Serniak, M. Hays, G. de Lange, S. Diamond, S. Shankar, L. D. Burkhart, L. Frunzio, M. Houzet, and M. H. Devoret, Hot Nonequilibrium Quasiparticles in Transmon Qubits, Phys. Rev. Lett. **121**, 157701 (2018), publisher: American Physical Society.

[2] A. P. Vepsäläinen, A. H. Karamlou, J. L. Orrell, A. S. Dogra, B. Loer, F. Vasconcelos, D. K. Kim, A. J. Melville, B. M. Niedzielski, J. L. Yoder, S. Gustavsson, J. A. Formaggio, B. A. VanDevender, and W. D. Oliver, Impact of ionizing radiation on superconducting qubit coherence, Nature **584**, 551 (2020), number: 7822 Publisher: Nature Publishing Group.

[3] C. D. Wilen, S. Abdullah, N. A. Kurinsky, C. Stanford, L. Cardani, G. D'Imperio, C. Tomei, L. Faoro, L. B. Ioffe, C. H. Liu, A. Opremcak, B. G. Christensen, J. L. DuBois, and R. McDermott, Correlated charge noise and relaxation errors in superconducting qubits, Nature **594**, 369 (2021), number: 7863 Publisher: Nature Publishing Group.

[4] J. M. Martinis, Saving superconducting quantum processors from decay and correlated errors generated by gamma and cosmic rays, npj Quantum Inf **7**, 1 (2021), number: 1 Publisher: Nature Publishing Group.

[5] R. Barends, J. Wenner, M. Lenander, Y. Chen, R. C. Bialczak, J. Kelly, E. Lucero, P. O'Malley, M. Mariantoni, D. Sank, H. Wang, T. C. White, Y. Yin, J. Zhao, A. N. Cleland, J. M. Martinis, and J. J. A. Baselmans, Minimizing quasiparticle generation from stray infrared light in superconducting quantum circuits, Appl. Phys. Lett. **99**, 113507 (2011), publisher: American Institute of Physics.

[6] P. J. de Visser, J. J. A. Baselmans, P. Diener, S. J. C. Yates, A. Endo, and T. M. Klapwijk, Number Fluctuations of Sparse Quasiparticles in a Superconductor, Phys. Rev. Lett. **106**, 167004 (2011), publisher: American Physical Society.

[7] K. Serniak, S. Diamond, M. Hays, V. Fatemi, S. Shankar, L. Frunzio, R. J. Schoelkopf, and M. H. Devoret, Direct Dispersive Monitoring of Charge Parity in Offset-Charge-Sensitive Transmons, Phys. Rev. Applied **12**, 014052 (2019), publisher: American Physical Society.

[8] E. T. Mannila, P. Samuelsson, S. Simbierowicz, J. T. Peltonen, V. Vesterinen, L. Grönberg, J. Hassel, V. F. Maisi, and J. P. Pekola, A superconductor free of quasiparticles for seconds, Nat. Phys. **18**, 145 (2022), number: 2 Publisher: Nature Publishing Group.

[9] A. D. Córcoles, J. M. Chow, J. M. Gambetta, C. Rigetti, J. R. Rozen, G. A. Keefe, M. Beth Rothwell, M. B. Ketchen, and M. Steffen, Protecting superconducting qubits from radiation, Appl. Phys. Lett. **99**, 181906 (2011), publisher: American Institute of Physics.

[10] I. M. Pop, K. Geerlings, G. Catelani, R. J. Schoelkopf, L. I. Glazman, and M. H. Devoret, Coherent suppression of electromagnetic dissipation due to superconducting quasiparticles, Nature **508**, 369 (2014), number: 7496 Publisher: Nature Publishing Group.

[11] N. A. Court, A. J. Ferguson, R. Lutchyn, and R. G. Clark, Quantitative study of quasiparticle traps using the single-cooper-pair transistor, Phys. Rev. B **77**, 100501 (2008).

[12] R.-P. Riwar, A. Hosseinkhani, L. D. Burkhart, Y. Y. Gao, R. J. Schoelkopf, L. I. Glazman, and G. Catelani, Normal-metal quasiparticle traps for superconducting qubits, Phys. Rev. B **94**, 104516 (2016), publisher: American Physical Society.

[13] F. Henriques, F. Valenti, T. Charpentier, M. Lagoin, C. Gouriou, M. Martínez, L. Cardani, M. Vignati, L. Grünhaupt, D. Gusenkova, J. Ferrero, S. T. Skacel, W. Wernsdorfer, A. V. Ustinov, G. Catelani, O. Sander, and I. M. Pop, Phonon traps reduce the quasiparticle density in superconducting circuits, Appl. Phys. Lett. **115**, 212601 (2019), publisher: American Institute of Physics.

[14] O. Rafferty, S. Patel, C. H. Liu, S. Abdullah, C. D. Wilen, D. C. Harrison, and R. McDermott, Spurious Antenna Modes of the Transmon Qubit (2021), arXiv:2103.06803 [cond-mat, physics:quant-ph].

[15] C. Kurter, C. E. Murray, R. T. Gordon, B. B. Wymore, M. Sandberg, R. M. Shelby, A. Eddins, V. P. Adiga, A. D. K. Finck, E. Rivera, A. A. Stabile, B. Trimm, B. Wacaser, K. Balakrishnan, A. Pyzyna, J. Sleight, M. Steffen, and K. Rodbell, Quasiparticle tunneling as a probe of Josephson junction barrier and capacitor material in superconducting qubits, npj Quantum Inf **8**, 1 (2022), number: 1 Publisher: Nature Publishing Group.

[16] X. Pan, H. Yuan, Y. Zhou, L. Zhang, J. Li, S. Liu, Z. H. Jiang, G. Catelani, L. Hu, and F. Yan, Engineering superconducting qubits to reduce quasiparticles and charge noise (2022), arXiv:2202.01435 [cond-mat, physics:quant-ph].

[17] A. Bargerbos, L. J. Splitthoff, M. Pita-Vidal, J. J. Wesdorp, Y. Liu, P. Krogstrup, L. P. Kouwenhoven, C. K. Andersen, and L. Grünhaupt, Mitigation of quasiparticle loss in superconducting qubits by phonon scattering

(2022), arXiv:2207.12754 [cond-mat, physics:quant-ph].
[18] J. Aumentado, M. W. Keller, J. M. Martinis, and M. H. Devoret, Nonequilibrium Quasiparticles and $2e$ Periodicity in Single-Cooper-Pair Transistors, Phys. Rev. Lett. **92**, 066802 (2004), publisher: American Physical Society.
[19] O. Naaman and J. Aumentado, Time-domain measurements of quasiparticle tunneling rates in a single-Cooper-pair transistor, Phys. Rev. B **73**, 172504 (2006), publisher: American Physical Society.
[20] R. M. Lutchyn and L. I. Glazman, Kinetics of quasiparticle trapping in a Cooper-pair box, Phys. Rev. B **75**, 184520 (2007), publisher: American Physical Society.
[21] M. D. Shaw, R. M. Lutchyn, P. Delsing, and P. M. Echternach, Kinetics of nonequilibrium quasiparticle tunneling in superconducting charge qubits, Phys. Rev. B **78**, 024503 (2008), publisher: American Physical Society.
[22] L. Sun, L. DiCarlo, M. D. Reed, G. Catelani, L. S. Bishop, D. I. Schuster, B. R. Johnson, G. A. Yang, L. Frunzio, L. Glazman, M. H. Devoret, and R. J. Schoelkopf, Measurements of Quasiparticle Tunneling Dynamics in a Band-Gap-Engineered Transmon Qubit, Phys. Rev. Lett. **108**, 230509 (2012), publisher: American Physical Society.
[23] M. Zgirski, L. Bretheau, Q. Le Masne, H. Pothier, D. Esteve, and C. Urbina, Evidence for Long-Lived Quasiparticles Trapped in Superconducting Point Contacts, Phys. Rev. Lett. **106**, 257003 (2011), publisher: American Physical Society.
[24] E. Levenson-Falk, F. Kos, R. Vijay, L. Glazman, and I. Siddiqi, Single-Quasiparticle Trapping in Aluminum Nanobridge Josephson Junctions, Phys. Rev. Lett. **112**, 047002 (2014), publisher: American Physical Society.
[25] D. G. Olivares, A. L. Yeyati, L. Bretheau, Ç. Ö. Girit, H. Pothier, and C. Urbina, Dynamics of quasiparticle trapping in Andreev levels, Phys. Rev. B **89**, 104504 (2014), publisher: American Physical Society.
[26] M. Hays, G. de Lange, K. Serniak, D. J. van Woerkom, D. Bouman, P. Krogstrup, J. Nygård, A. Geresdi, and M. H. Devoret, Direct Microwave Measurement of Andreev-Bound-State Dynamics in a Semiconductor-Nanowire Josephson Junction, Phys. Rev. Lett. **121**, 047001 (2018), publisher: American Physical Society.
[27] J. T. Farmer, A. Zarassi, D. M. Hartsell, E. Vlachos, H. Zhang, and E. M. Levenson-Falk, Continuous real-time detection of quasiparticle trapping in aluminum nanobridge Josephson junctions, Appl. Phys. Lett. **119**, 122601 (2021), publisher: American Institute of Physics.
[28] C. Janvier, L. Tosi, L. Bretheau, Ç. Ö. Girit, M. Stern, P. Bertet, P. Joyez, D. Vion, D. Esteve, M. F. Goffman, H. Pothier, and C. Urbina, Coherent manipulation of Andreev states in superconducting atomic contacts, Science **349**, 1199 (2015), publisher: American Association for the Advancement of Science.
[29] M. Hays, V. Fatemi, D. Bouman, J. Cerrillo, S. Diamond, K. Serniak, T. Connolly, P. Krogstrup, J. Nygård, A. Levy Yeyati, A. Geresdi, and M. H. Devoret, Coherent manipulation of an Andreev spin qubit, Science **373**, 430 (2021), publisher: American Association for the Advancement of Science.
[30] R. Vijay, J. D. Sau, M. L. Cohen, and I. Siddiqi, Optimizing Anharmonicity in Nanoscale Weak Link Josephson Junction Oscillators, Phys. Rev. Lett. **103**, 087003 (2009), publisher: American Physical Society.
[31] R. Vijay, E. M. Levenson-Falk, D. H. Slichter, and I. Siddiqi, Approaching ideal weak link behavior with three dimensional aluminum nanobridges, Appl. Phys. Lett. **96**, 223112 (2010), publisher: American Institute of Physics.
[32] E. M. Levenson-Falk, R. Vijay, and I. Siddiqi, Nonlinear microwave response of aluminum weak-link Josephson oscillators, Appl. Phys. Lett. **98**, 123115 (2011), publisher: American Institute of Physics.
[33] I. O. Kulik and A. N. Omel'Yanchuk, Contribution to the microscopic theory of the Josephson effect in superconducting bridges, ZhETF Pisma Redaktsiiu **21**, 216 (1975), aDS Bibcode: 1975ZhPmR..21..216K.
[34] O. N. Dorokhov, Transmission coefficient and the localization length of an electron in N bound disordered chains, Soviet Journal of Experimental and Theoretical Physics Letters **36**, 318 (1982), aDS Bibcode: 1982JETPL..36..318D.
[35] See supplemental material at [url] for the full experimental diagram, detailed derivation of models, and intermediate fitting procedures.
[36] hmmlearn — hmmlearn 0.2.8 documentation.
[37] L. Rabiner, A tutorial on hidden Markov models and selected applications in speech recognition, Proceedings of the IEEE **77**, 257 (1989), conference Name: Proceedings of the IEEE.
[38] M. J. Persky, Review of black surfaces for space-borne infrared systems, Review of Scientific Instruments **70**, 2193 (1999), publisher: American Institute of Physics.
[39] T. Connolly, P. D. Kurilovich, S. Diamond, H. Nho, C. G. Bøttcher, L. I. Glazman, V. Fatemi, and M. H. Devoret, Coexistence of nonequilibrium density and equilibrium energy distribution of quasiparticles in a superconducting qubit, arXiv preprint arXiv:2302.12330 (2023).
[40] R. Anthony-Petersen, A. Biekert, R. Bunker, C. L. Chang, Y.-Y. Chang, L. Chaplinsky, E. Fascione, C. W. Fink, M. Garcia-Sciveres, R. Germond, W. Guo, S. A. Hertel, Z. Hong, N. Kurinsky, X. Li, J. Lin, M. Lisovenko, R. Mahapatra, A. Mayer, D. McKinsey, S. Mehrotra, N. Mirabolfathi, B. Neblosky, W. A. Page, P. K. Patel, B. Penning, H. D. Pinckney, M. Platt, M. Pyle, M. Reed, R. K. Romani, H. S. Queiroz, B. Sadoulet, B. Serfass, R. Smith, P. F. Sorensen, B. Suerfu, A. Suzuki, R. Underwood, V. Velan, G. Wang, Y. Wang, S. L. Watkins, M. R. Williams, V. Yefremenko, and J. Zhang, A Stress Induced Source of Phonon Bursts and Quasiparticle Poisoning (2022), arXiv:2208.02790 [cond-mat, physics:physics].
[41] L. Cardani, F. Valenti, N. Casali, G. Catelani, T. Charpentier, M. Clemenza, I. Colantoni, A. Cruciani, G. D'Imperio, L. Gironi, L. Grünhaupt, D. Gusenkova, F. Henriques, M. Lagoin, M. Martinez, G. Pettinari, C. Rusconi, O. Sander, C. Tomei, A. V. Ustinov, M. Weber, W. Wernsdorfer, M. Vignati, S. Pirro, and I. M. Pop, Reducing the impact of radioactivity on quantum circuits in a deep-underground facility, Nat Commun **12**, 2733 (2021), number: 1 Publisher: Nature Publishing Group.
[42] S. Diamond, V. Fatemi, M. Hays, H. Nho, P. D. Kurilovich, T. Connolly, V. R. Joshi, K. Serniak, L. Frunzio, L. I. Glazman, and M. H. Devoret, Distinguishing Parity-Switching Mechanisms in a Superconducting Qubit, PRX Quantum **3**, 040304 (2022), publisher: American Physical Society.